AIAA JOURNAL
Vol. 36, No. 12, December 1998

Adaptive Finite Element Solution of Compressible Turbulent Flows

F. Ilinca*
National Research Council of Canada, Boucherville, Québec J4B 6Y4, Canada
and
D. Pelletier† and L. Ignat‡
École Polytechnique de Montréal, Montréal, Québec H3C 3A7, Canada

An adaptive finite element method for solving compressible turbulent flows up to transonic regime is presented. Pressure-based methods previously developed for laminar compressible flows and turbulent incompressible flows are combined to solve compressible turbulent flows. Turbulence is incorporated via the k–ϵ model. The algorithm uses the logarithms of k and ϵ as computational variables to preserve positivity. Solutions are obtained in primitive variables using quadratic finite elements on unstructured grids. The error is estimated by a local projection method. The solution algorithm and error estimation are validated on problems with known analytical solutions. The method is then applied to compressible subsonic and transonic flows and predictions are compared with experimental measurements.

Nomenclature

c_p = specific heat
E = roughness parameter
$\mathcal{E}$ = natural logarithm of ϵ
$\boldsymbol{f}$ = body force
$\boldsymbol{I}$ = identity matrix
$\mathcal{K}$ = natural logarithm of the turbulence kinetic energy (TKE)
k = TKE
M = Mach number
Pr = Prandtl number, $(\mu c_p)/\lambda$
$P(\boldsymbol{u})$ = production term
p = pressure
q_s = heat source
R = thermodynamic gas constant
Re = Reynolds number, $(\rho U L)/\mu$
T = temperature
$\boldsymbol{u}$ = velocity vector
$\dot{\gamma}$ = strain rate tensor
ϵ = turbulence dissipation rate
κ = von Kármán constant
λ = thermal conductivity
μ = viscosity
ρ = density
τ = stress tensor
∇ = gradient operator
$\nabla\cdot$ = divergence

Subscripts

T = turbulent
w = values on the boundary

I. Introduction

THE numerical simulation of compressible viscous flows in aerodynamics results in a tightly coupled system of nonlinear equations in which parameters often take extreme values. Such problems place special demands on the solution algorithm. Flow features such as boundary and shear layers, recirculation zones, and shock waves need to be properly resolved to achieve an accurate solution. Furthermore, in many cases it is difficult to determine a priori where the mesh must be refined to accurately capture the physics of the flow.

The method presented here is aimed at flow problems where incompressibility plays a key role. For example, an airfoil at takeoff conditions is characterized by an upstream Mach number in the vicinity of 0.3, the upper end of the incompressible flow regime. However, the flow over the airfoil may reach local Mach numbers as high as 0.6–0.7. As another example, consider a pressure vessel filled with a highly pressurized gas subject to a small local failure. The flow may reach the speed of sound as the tank is vented into its still surroundings. Viscous flows spanning this compressibility range are notoriously difficult to solve with density-based methods. Much effort has been devoted at preconditioning density-based methods with some success.[1] However, pressure-based methods are ideally suited for the incompressible flow regime. Such a method has been retained for the present study. The price to be paid is that the formulation is nonconservative so that shock strength predictions may be less accurate than those obtained by a density-based method. In primitive variables, the jump at the shock is accurate to the truncation error of the scheme.

Two-equation models with wall functions are powerful tools for solving complex turbulent flows because they provide good predictions at low cost. There is even a renewal of interest for wall functions because of their cost effectiveness.[2–4] One major hurdle in the numerical treatment of two-equation models lies in ensuring that the turbulence variables (here k and ϵ) remain positive throughout the flow domain and during the course of iterations. Failure to ensure this realizability condition can have devastating effects on the solution process. The eddy viscosity may locally become negative and result in immediate and irrecoverable breakdown of iterations.

Most positivity promoting algorithms are developed on a case by case basis because their design depends in part on the details of the turbulence model being used. The use of solution clipping and limiters is very widespread because of their robustness. However, using solution clipping and limiters does have two drawbacks. First, the convergence of the solver is slowed down because clipped values of the solution destroy the solution residuals. Second, clipping introduces noise and oscillations in the solution fields. Negative values that are locally reset to some small positive values can result in locally very large solution gradients, and hence large curvature, even if the values of k and ϵ are small. This is extremely detrimental

Presented as Paper 98-0229 at the AIAA 36th Aerospace Sciences Meeting and Exhibit, Reno, NV, Jan. 12–15, 1998; received Feb. 26, 1998; revision received Aug. 10, 1998; accepted for publication Aug. 10, 1998.

*Research Officer, Process Modeling and Optimization, Industrial Materials Institute, 75, de Mortagne.
†Professor, Department of Mechanical Engineering, C.P. 6079, Succ. A. Associate Fellow AIAA.
‡Graduate Research Assistant, Department of Mechanical Engineering, C.P. 6079, Succ. A.

to adaptive solution algorithms because they tend to cluster grid points in these regions. The net result is that the mesh is being adapted to the inability of the solver to produce a smooth and positive solution, rather than refining the grid in regions of large solution curvature. Solving for the natural logarithm of turbulence quantities is proposed in Refs. 5 and 6. This results in improved solution smoothness so that quantitative improvements by adaptive remeshing can be fully realized. This choice has several important advantages. Turbulence variables and source terms are all strictly positive throughout the domain. The change of variables also results in improved accuracy in regions of rapid variation of turbulence fields such as boundary layers, stagnation points, and shear layers, or in regions of very low-turbulence levels. This approach is also applicable to compressible flows and is effective for all two-equation models of turbulence.[7] Luo et al.[8] have implemented this approach in a density-based solver, and they report encouraging results. However, no adaptivity was used.

Initial success with adaptive methods were achieved in transonic Euler flows because of the pressing need for accurate shock predictions.[9] A simple and popular approach consists in clustering points in regions of large gradients of a key variable such as density or Mach number.[10] Although effective for Euler flows, the method does not perform as well for viscous flows. Such methods experience difficulties in detecting both shocks and boundary layers. This is not surprising because the two phenomena are characterized by different physics. An error estimator of this kind, designed for anisotropic adaptation and compressible flows, was presented by Fortin et al.[11] It is based on the evaluation of the second derivatives of density and is restricted to linear elements. The present work uses quadratic elements. Furthermore, in the present case, the tight coupling between all flow variables requires computation of error estimates for all dependent variables. Recently, Becker and Rannacher[12] developed a family of estimators based on the solution of a dual problem for the error. The method was developed for a linear problem and a Galerkin finite element method. Extensions to nonlinear problems and/or stabilized finite element techniques is a nontrivial issue. Zienkiewicz and Zhu[13] proposed a postprocessing error estimator based on projection. Essentially, the method consists in constructing smooth continuous derivatives by a least-squares projection of the discontinuous finite element derivatives. The error is then evaluated by computing the difference between the recovered derivatives and finite element derivatives using an energy norm. This method was used by Wu et al.[14] to estimate error for transient solutions of the incompressible Navier–Stokes equations. Recent work reports improvement in the accuracy of the recovered derivatives. Zienkiewicz and Zhu[15] presented a local recovery technique that yields very good results. Analyses of the Zienkiewicz–Zhu global flux projection estimator were performed by Ainsworth et al.[16] and Ainsworth and Oden.[17] Results show that, even if the basis of the estimator is heuristic, the method produces good estimates of the error.

The methodology presented here is based on adaptive remeshing coupled to a finite element solver for steady-state compressible turbulent flows. Turbulence is modeled using the standard k–ϵ model of Launder and Spalding.[18] Turbulence equations are written in terms of the logarithms of k and ϵ following Ilinca[5] and Ilinca and Pelletier.[6] Error estimates are obtained by a local projection method. The remeshing procedure makes it possible to easily perform adaptive grid refinement studies so that grid independent predictions are obtained.[6,7] In Refs. 19 and 20, Ilinca and Pelletier have demonstrated the methodology on compressible laminar flows with known analytical solution and by computing cases for which experimental measurements were available. The methodology was also applied to zero- and two-equation models of turbulence for incompressible flows.[21–24] Here we present an extension of the methodology to compressible turbulent flows.

The focus of the present work is on demonstrating how adaptivity can produce grid-independent predictions for two-equation models of turbulence in compressible flows. We restrict ourselves to subsonic and transonic regimes. The method presented could be extended to supersonic flows. This would require changes in the flow solver to handle boundary conditions for supersonic flows and modifications in the turbulence model to account for compressibility effects, for instance, see Ref. 25 or 26.

The paper is organized as follows. Section II presents the compressible Reynolds-averaged Navier–Stokes equations and the turbulence equations for the standard k–ϵ model of Launder and Spalding.[18] Section III discusses the change of variables leading to the logarithmic form of the turbulence equations and some of the advantages of using such variables. The solution algorithm is discussed in Sec. IV. Section V summarizes the finite element formulation used to solve the differential equations. The error estimation and adaptive strategies used in conjunction with the new variables are reviewed. Section VI presents results obtained on problems for which closed-form solutions or experimental data are available. The paper ends with conclusions.

II. Modeling of the Problem

A. Flow Equations

The flow regime of interest is modeled by the Reynolds-averaged Navier–Stokes and energy equations

$$\rho \boldsymbol{u}\cdot\nabla\boldsymbol{u} = -\nabla p + \nabla\cdot\left[(\mu+\mu_T)\left(\nabla\boldsymbol{u}+\nabla\boldsymbol{u}^T-\tfrac{2}{3}\boldsymbol{I}\nabla\cdot\boldsymbol{u}\right)\right]+\rho\boldsymbol{f} \tag{1}$$

$$-\nabla\cdot\boldsymbol{u} = (1/\rho)(\boldsymbol{u}\cdot\nabla)\rho \tag{2}$$

$$\rho c_p \boldsymbol{u}\cdot\nabla T = \boldsymbol{u}\cdot\nabla p + \nabla\cdot[(\lambda+\lambda_T)\nabla T]+\rho q_s \tag{3}$$

where μ is the fluid viscosity. In addition, the equation of state relates density to pressure and temperature by

$$\rho = p/RT \tag{4}$$

The preceding equations are solved in the following dimensionless form (for details see Ref. 20):

$$\tilde{\rho}\tilde{\boldsymbol{u}}\cdot\tilde{\nabla}\tilde{\boldsymbol{u}} = -\tilde{\nabla}\tilde{p} + \tilde{\nabla}\cdot\left[(\tilde{\mu}+\tilde{\mu}_T)\left(\tilde{\nabla}\tilde{\boldsymbol{u}}+\tilde{\nabla}\tilde{\boldsymbol{u}}^T-\tfrac{2}{3}\boldsymbol{I}\tilde{\nabla}\cdot\tilde{\boldsymbol{u}}\right)\right]+\tilde{\rho}\tilde{\boldsymbol{f}} \tag{5}$$

$$-\tilde{\nabla}\cdot\tilde{\boldsymbol{u}} = \frac{\gamma M_\infty^2}{\gamma M_\infty^2\tilde{p}+1}(\tilde{\boldsymbol{u}}\cdot\tilde{\nabla})\tilde{p} - \frac{1}{\tilde{T}}(\tilde{\boldsymbol{u}}\cdot\tilde{\nabla})\tilde{T} \tag{6}$$

$$\tilde{\rho}\tilde{c}_p\tilde{\boldsymbol{u}}\cdot\tilde{\nabla}\tilde{T} = (\gamma-1)M_\infty^2\tilde{\boldsymbol{u}}\cdot\tilde{\nabla}\tilde{p} + \tilde{\nabla}\cdot[(\tilde{\lambda}+\tilde{\lambda}_T)\tilde{\nabla}\tilde{T}]+\tilde{\rho}\tilde{q}_s \tag{7}$$

$$\tilde{\rho} = \frac{\gamma M_\infty^2\tilde{p}+1}{\tilde{T}} \tag{8}$$

The dimensionless variables are defined as

$$\tilde{u} = \frac{u}{U_\infty},\qquad \tilde{T} = \frac{T}{T_\infty},\qquad \tilde{p} = \frac{p}{\rho_\infty U_\infty^2} - \frac{1}{\gamma M_\infty^2}$$

$$M_\infty = \frac{U_\infty}{\sqrt{\gamma RT_\infty}},\qquad \tilde{f} = \frac{fL}{U_\infty^2},\qquad \tilde{q}_s = \frac{q_s L}{c_p U_\infty T_\infty},\qquad \tilde{\rho} = \frac{\rho}{\rho_\infty} \tag{9}$$

$$\tilde{c}_p = 1,\qquad \tilde{\mu} = \frac{1}{Re} = \frac{\mu}{\rho_\infty U_\infty L},\qquad \tilde{\mu}_T = \frac{1}{Re_T} = \frac{\mu_T}{\rho_\infty U_\infty L}$$

$$\tilde{\lambda} = \frac{1}{PrRe} = \frac{\lambda}{\rho_\infty c_p U_\infty L},\qquad \tilde{\lambda}_T = \frac{1}{Pr_T Re_T} = \frac{\lambda_T}{\rho_\infty c_p U_\infty L}$$

where subscript ∞ denotes a freestream variable and L is a reference length.

As can be seen, this set of equations is perfectly well suited for both compressible and incompressible flows. The Mach number identifies the compressibility effects due to pressure. Therefore, when $M_\infty = 0$, there are no density variations induced by the pressure and no compressibility terms in the continuity and energy equations. Moreover, without heat sources or heated walls, the flow will be isothermal. Hence, density will be constant, and the flow will be divergence free. If M_∞ equals zero and walls are heated, the equations for variable density (anelastic) flows are recovered with the proper equation of state.

The turbulent viscosity μ_T and the turbulent thermal conductivity λ_T are computed using the k–ϵ model of turbulence. In this model, the turbulence quantities are the turbulence kinetic energy k and its

dissipation rate ϵ, which are governed by the following transport equations[18]:

$$\rho \boldsymbol{u} \cdot \nabla k = \nabla \cdot \{[\mu + (\mu_T/\sigma_k)]\nabla k\} + \left[\mu_T P(\boldsymbol{u}) - \tfrac{2}{3}\rho k \nabla \cdot \boldsymbol{u}\right] - \rho\epsilon \tag{10}$$

$$\rho \boldsymbol{u} \cdot \nabla \epsilon = \nabla \cdot \{[\mu + (\mu_T/\sigma_\epsilon)]\nabla \epsilon\} + C_{\epsilon 1}(\epsilon/k)\left[\mu_T P(\boldsymbol{u}) - \tfrac{2}{3}\rho k \nabla \cdot \boldsymbol{u}\right] - C_{\epsilon 2}\rho(\epsilon^2/k) \tag{11}$$

where the production of turbulence is defined as

$$P(\boldsymbol{u}) = \nabla \boldsymbol{u} : \left[(\nabla \boldsymbol{u} + \nabla \boldsymbol{u}^T) - \tfrac{2}{3}\boldsymbol{I}\nabla \cdot \boldsymbol{u}\right] \tag{12}$$

The eddy viscosity and thermal conductivity are computed from k and ϵ by

$$\mu_T = \rho C_\mu (k^2/\epsilon) \tag{13}$$

$$\lambda_T = \mu_T c_p / Pr_T \tag{14}$$

with the turbulent Prandtl number Pr_T equal to unity. The constants σ_k, σ_ϵ, $C_{\epsilon 1}$, $C_{\epsilon 2}$, and C_μ take the standard values proposed by Launder and Spalding[18]:

$$\sigma_k = 1.0, \qquad \sigma_\epsilon = 1.3, \qquad C_{\epsilon 1} = 1.44$$
$$C_{\epsilon 2} = 1.92, \qquad C_\mu = 0.09 \tag{15}$$

B. Wall Boundary Conditions

On the boundary a combination of Neumann and Dirichlet conditions are imposed using wall functions, which describe the asymptotic behavior of the different variables near a solid wall.[18] The normal derivative of the turbulent kinetic energy (TKE) is set to zero near the wall. The TKE values at boundary points k_w are computed implicitly. The value of the wall shear stress is then given by

$$\tau_w = \frac{\rho U C_\mu^{\frac{1}{4}} k_w^{\frac{1}{2}}}{U^+} \tag{16}$$

where

$$U^+ = \begin{cases} y^+, & y^+ < y_c^+ \\ 1/\kappa\, \ell n(E y^+), & y^+ \geq y_c^+ \end{cases} \tag{17}$$

$$y^+ = \frac{\rho C_\mu^{\frac{1}{4}} k_w^{\frac{1}{2}} y}{\mu} \tag{18}$$

Here y is the distance between the computational boundary and the wall, and roughness parameter $E = 9.0$ for smooth walls.

For temperature, boundary conditions at the wall may be enforced by using a temperature wall function. The procedure is then similar to that used for the momentum equations.[27,28] However, in the present applications the walls are adiabatic so that the wall heat flux q_w is zero.

Finally, TKE dissipation at boundary points is obtained by using

$$\epsilon_w = \frac{C_\mu^{\frac{3}{4}} k_w^{\frac{3}{2}}}{\kappa y} \tag{19}$$

III. Logarithmic Form of the Turbulence Equations

Although mathematically correct, the turbulence equations in the Sec. II may lead to difficulties in the numerical solution algorithm. For example, the eddy viscosity may become negative in some cases if ϵ becomes negative. This will cause a dramatic breakdown of the solution algorithm. Also, several source terms contain division by the value of one turbulence variable (k, for example). Negative or small values of the denominator can lead to improper sign or overly large values. Enhanced robustness of the algorithm will be achieved if one can ensure that turbulence variables remain positive throughout the domain and during the course of iterations.

One way to preserve positivity of the dependent variables consists in solving for their logarithms[5,6]:

$$\mathcal{K} = \ell n(k), \qquad \mathcal{E} = \ell n(\epsilon) \tag{20}$$

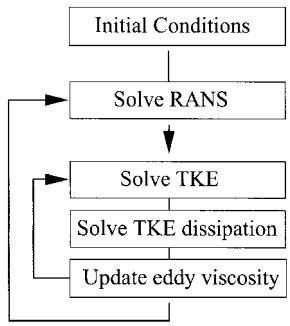

Fig. 1 Solution algorithm.

Solving for $\mathcal{K}$ and $\mathcal{E}$ guarantees that k and ϵ will remain positive throughout the computations. Hence, the eddy viscosity μ_T will always remain positive.

The turbulence equations and the eddy viscosity definition for logarithmic variables are given by

$$\rho \boldsymbol{u} \cdot \nabla \mathcal{K} = \nabla \cdot \{[\mu + (\mu_T/\sigma_k)]\nabla \mathcal{K}\} + [\mu + (\mu_T/\sigma_k)](\nabla \mathcal{K})^2 + \left[\mu_T e^{-\mathcal{K}} P(\boldsymbol{u}) - \tfrac{2}{3}\rho \nabla \cdot \boldsymbol{u}\right] - \rho\, e^{\mathcal{E}-\mathcal{K}} \tag{21}$$

$$\rho \boldsymbol{u} \cdot \nabla \mathcal{E} = \nabla \cdot \{[\mu + (\mu_T/\sigma_\epsilon)]\nabla \mathcal{E}\} + [\mu + (\mu_T/\sigma_\epsilon)](\nabla \mathcal{E})^2 + C_{\epsilon 1}\left[\mu_T e^{-\mathcal{K}} P(\boldsymbol{u}) - \tfrac{2}{3}\rho \nabla \cdot \boldsymbol{u}\right] - C_{\epsilon 2}\rho\, e^{\mathcal{E}-\mathcal{K}} \tag{22}$$

$$\mu_T = \rho C_\mu\, e^{2\mathcal{K}-\mathcal{E}} \tag{23}$$

Note that the equations for logarithmic variables are equivalent to the original equations of the turbulence model. Hence, there is no change in the turbulence model. The only difference is that the computational variables are now the logarithms of the turbulence quantities; see Refs. 5 and 6 for details.

IV. Solution Algorithm

The momentum, continuity, and energy equations are solved in a fully coupled manner, by expressing density as a function of pressure and temperature.[19,20] Linearization is performed with Newton's method. For the k–ϵ model, a robust finite element scheme is obtained by rewriting the equations for k and ϵ in block triangular form using the eddy viscosity definition.[6,22] The global system of equations is solved in a partly segregated manner, as shown in Fig. 1.

The momentum, energy, and turbulence transport equations are dominated by convection, and it is well known that a standard Galerkin discretization leads to oscillations in the solution. Hence, some form of upwinding is required to suppress these nonphysical oscillations. Here we use a variant of the streamline-upwind/Petrov–Galerkin method as detailed in Refs. 5 and 20. The equations are discretized using a six-node triangular element, which uses a linear continuous pressure and a quadratic interpolant for velocity, temperature, and turbulence variables.

V. Adaptive Methodology

Adaptive methods are now well recognized as means of improving solution accuracy and flow resolution. References 9, 29, and 30 present typical examples of adaptive remeshing, h-refinement, nodal relocation, and p-enrichment methods. Adaptive remeshing has been retained for the present work because of its ability to easily provide very high and localized resolution of flow features.[21–23] In this approach, the problem is first solved on a coarse mesh. The global and local accuracy of the solution is estimated, and an improved mesh is generated with more elements where the solution is insufficiently accurate. The problem is solved again on the new mesh using the solution obtained on the previous mesh as an initial guess. The process is repeated until the required accuracy is achieved.

The key point in the adaptive process is the error estimation. From a practical point of view, the estimate of the error must reproduce the distribution of the exact error, indicating where the mesh must be refined to improve accuracy. The flow problem consists of solving a system of tightly coupled highly nonlinear differential equations: momentum, continuity, energy, turbulence equations, and state equation. The flow is at high Reynolds number, and the Mach

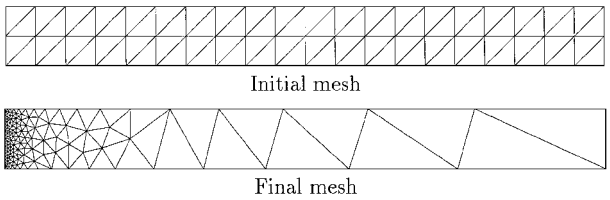

Fig. 2 Meshes for the analytical solution.

number ranges from the low-compressible or incompressible regime up to transonic speeds. The viscous terms are important in boundary layers, whereas away from the walls the flow is nearly inviscid. Therefore, the error estimator must be as general as possible. In this work, the error estimator is independent of the differential equations, of the solution algorithm, and of the finite element formulation. The main hypothesis is that derivatives of the exact solution are continuous throughout the computational domain. This is true away from shocks. The finite element derivatives are discontinuous across element faces. An approximation to the exact derivatives is obtained by a local least-squares projection of the finite element derivatives.[15] An error estimate is obtained by computing the norm of the difference between the reconstructed and finite element derivatives. The technique has already been described in details in previous papers[5,6,22–24]; hence, it is not repeated here. Thus, the estimator is not valid near shocks because the solution is discontinuous across a shock. Near shocks, the error estimator will always detect an error larger than the exact error. In fact, near a shock, the estimate of the error may become unbounded with mesh refinement even though the accuracy of the solution actually improves. This may result in excessive refinement near shocks and in an inaccurate global error estimate. To avoid this, we have used the technique proposed by de Sampaio et al.[31] to deal with singularities. Near shocks, a lower bound $h_{\min}$ is imposed on the mesh size. All elements for which the adaptive procedure prescribes a mesh size smaller than $h_{\min}$ are considered shock elements. For these elements, the mesh size for the adapted grid is set to $h_{\min}$, and their elemental contribution to the global error is discarded.[31]

Once the error estimates are obtained for all variables, there remains to design a better mesh. The adaptive remeshing procedure described previously in Refs. 5 and 6 is used to cluster grid points in regions of rapid variations of all field variables: velocity, pressure, temperature, logarithmic turbulence variables, and the eddy viscosity. The mesh characteristics (element size) are derived for each variable on a given element. The minimum element size predicted by each of the dependent variable is selected on each element. Details of this algorithm may be found in Refs. 5 and 6.

VI. Numerical Results

A. Turbulence Decay in an Uniform Flow

The performance of the logarithmic variables approach is illustrated on a simple but realistic problem with an analytical solution: the decay of grid turbulence. In a uniform flow, the production term vanishes in the turbulence equations. The diffusion terms are also neglected. Therefore, for $u = 1$ and $v = 0$, the turbulence equations reduce to[8]

$$\rho \frac{\partial k}{\partial x} = -\rho\epsilon \tag{24}$$

$$\rho \frac{\partial \epsilon}{\partial x} = -\rho C_{\epsilon 2} \frac{\epsilon^2}{k} \tag{25}$$

which have the following solution[8]:

$$k = \epsilon_0(\epsilon_0/k_0)^{-[C_{\epsilon 2}/(C_{\epsilon 2}-1)]}[(C_{\epsilon 2}-1)(x-x_0) + (k_0/\epsilon_0)]^{-[1/(C_{\epsilon 2}-1)]} \tag{26}$$

$$\epsilon = \epsilon_0(\epsilon_0/k_0)^{-[C_{\epsilon 2}/(C_{\epsilon 2}-1)]}[(C_{\epsilon 2}-1)(x-x_0) + (k_0/\epsilon_0)]^{-[C_{\epsilon 2}/(C_{\epsilon 2}-1)]} \tag{27}$$

where k_0 and ϵ_0 are the turbulence kinetic energy and the turbulence dissipation at $x = x_0$. The problem was solved on the rectangle $[0, 1] \times [0, 0.2]$. The turbulence variables at the inflow ($x_0 = 0$) are taken to be $k_0 = 1.0 \times 10^{-4}$ and $\epsilon_0 = 9.0 \times 10^{-3}$. This corresponds to a turbulence Reynolds number of 10^7.

Table 1 Trajectory of the error on $\mathcal{K}$

Mesh	Nodes	Elements	Error estimate	Effectivity index
0	205	80	1.437×10^{-1}	0.61
1	164	67	6.519×10^{-2}	0.63
2	142	61	1.082×10^{-1}	0.85
3	91	36	5.173×10^{-2}	0.80
4	125	52	3.560×10^{-2}	0.83
5	187	80	1.705×10^{-2}	0.80
6	259	112	1.357×10^{-2}	0.85
7	385	172	8.175×10^{-3}	0.92
8	533	240	5.285×10^{-3}	0.93

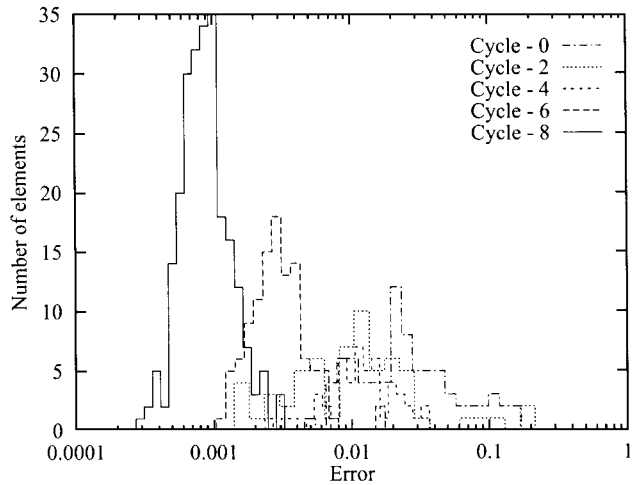

Fig. 3 Histogram of the elemental error.

The computation is initiated on an uniform mesh of 80 elements and 205 nodes. The meshes are then adapted to reduce the errors in the logarithmic variables and the eddy viscosity by a factor of two at each cycle of adaptation. The initial and final meshes are shown in Fig. 2. Table 1 summarizes the performance of the adaptive strategy for the error on the logarithm of k. As can be seen, in the first three cycles of adaptation the error diminishes even if the number of elements in the mesh decreases. This is possible because remeshing proceeds by a complete reallocation of grid points. Note that the error is reduced by a factor of 27 between the initial and final meshes. The last column shows the effectivity index of the estimator (ratio between the estimator and the true error). The effectivity index approaches one as the mesh is refined indicating that the accuracy of the estimator improves with mesh refinement. Similar results are obtained for ϵ. Figure 3 shows a typical histogram of the elemental error. It represents a count of the elements having the same level of error. In an ideal situation all elements would have the same error. In practice, we obtain a mesh with a clustering of elements near the average error. As can be seen from Fig. 3, the mean error is reduced throughout the domain. Furthermore, the proportion of the elements clustered near the mean increases from one cycle to the other indicating that the meshes tend toward optimality (the standard deviation decreases at each cycle). Note that mesh 4 contains fewer elements than meshes 0 and 2, but results in a more accurate solution because nodes are more efficiently distributed.

The numerical and exact solutions for ϵ and its logarithm are compared in Fig. 4. As can be seen, ϵ exhibits very rapid variations and takes very small values while $\mathcal{E}$ varies more slowly. Similar results are obtained for k and $\mathcal{K}$. This is an important source of numerical errors if the eddy viscosity is computed from k and ϵ because divisions by small numbers are performed. Logarithmic variables present gentler variations and result in a more accurate representation of the eddy viscosity. Note that there is little difference between the exact solution and the solution on the first adapted mesh.

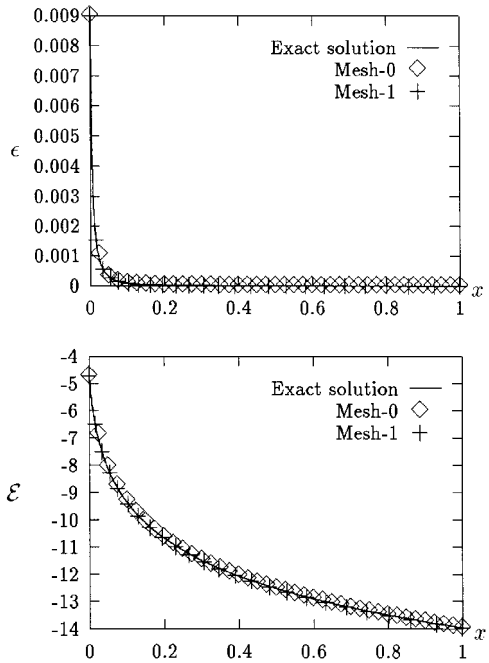

Fig. 4 Distribution of ϵ and $\mathcal{E}$.

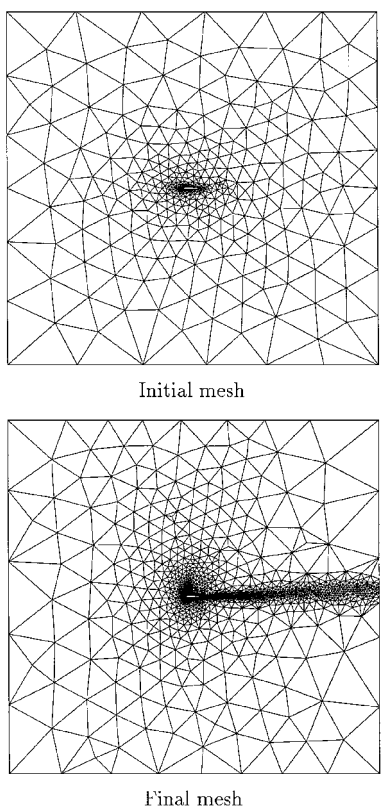

Fig. 5 NACA0012 airfoil.

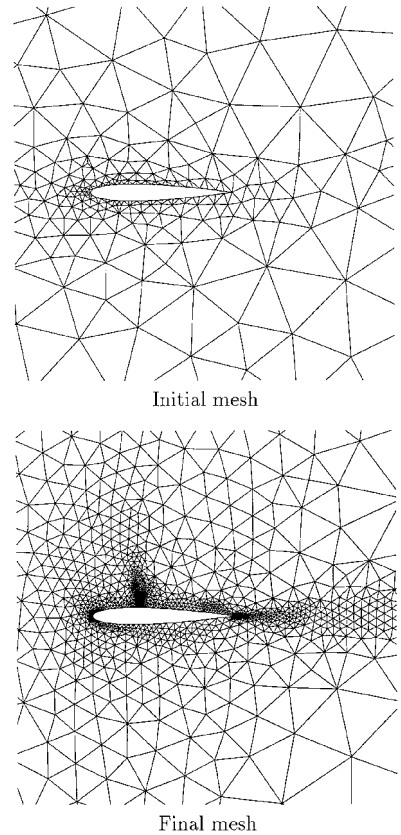

Fig. 6 Detail of the initial and final meshes near the airfoil.

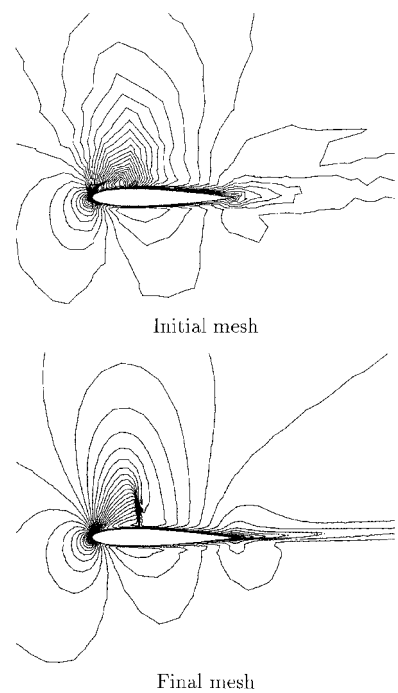

Fig. 7 Mach number distribution on the initial and final meshes.

Hence, subsequent adapted solutions are not shown because grid-independent predictions have been achieved. This improvement over previous results[8] is possibly due to the use of quadratic finite elements and adaptivity. We have tried to solve this problem with both the logarithmic variables approach and the standard procedure using k and ϵ. However, it was impossible to obtain converged solutions when equations were solved for k and ϵ, even when the initial guess was the solution obtained in logarithmic variables. This illustrates the increased robustness due to the use of logarithmic variables.

B. Transonic Turbulent Flow over an NACA0012 Airfoil at $M = 0.703$ and $\alpha = 3.22$ Degrees

Compressible turbulent flow over an NACA0012 airfoil at an angle of attack of 3.22 deg is computed at a Reynolds number of 1.8×10^6. The upstream Mach number is 0.703, which causes a shock to form on the upper side of the airfoil. The initial and final meshes obtained after three cycles of adaptation are shown in Fig. 5. As can be seen, the initial mesh is very coarse, whereas the final mesh is highly refined near the airfoil. Note also the mesh refinement in the wake of the airfoil. This is mostly due to the eddy viscosity error estimate. Figure 6 shows details of the mesh near the airfoil. The extreme clustering of grid points along the airfoil and near the shock is clearly seen. Figure 7 presents the Mach number contours obtained on these meshes. Figure 8 presents contours of the eddy viscosity near the airfoil. It is clear that the solution accuracy improves with mesh adaptation.

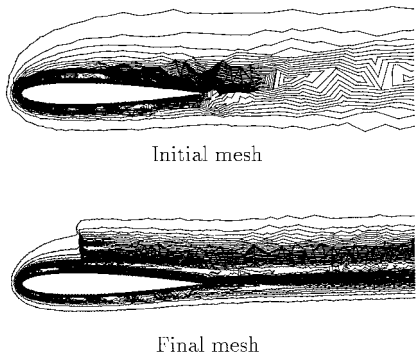

Fig. 8 Contours of the eddy viscosity.

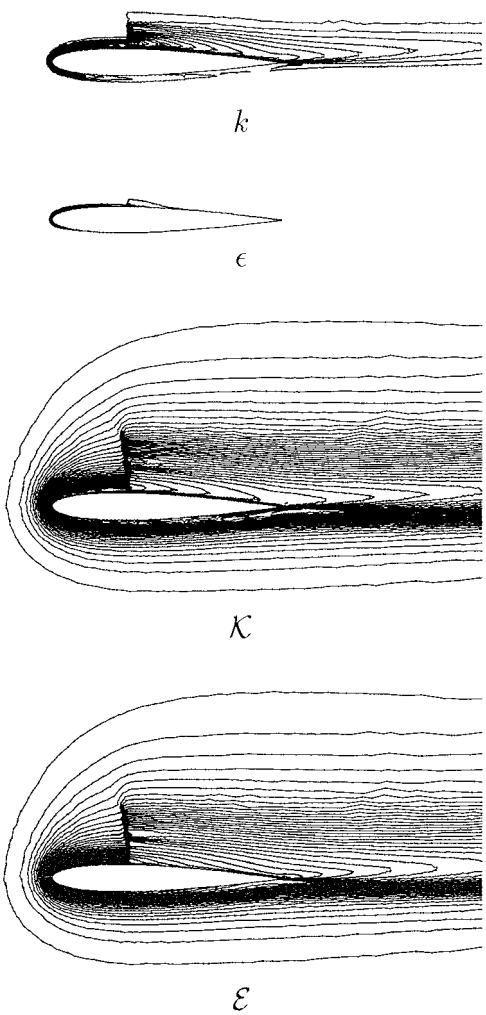

Fig. 9 Contours of k, ϵ, and logarithmic variables on the final mesh.

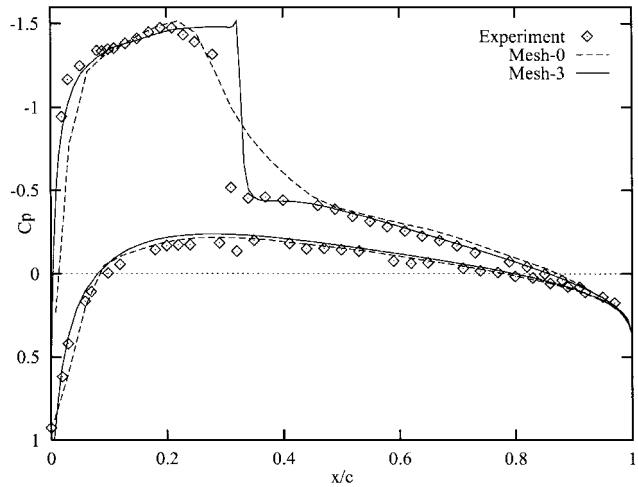

Fig. 10 Distribution of the pressure coefficient on the airfoil.

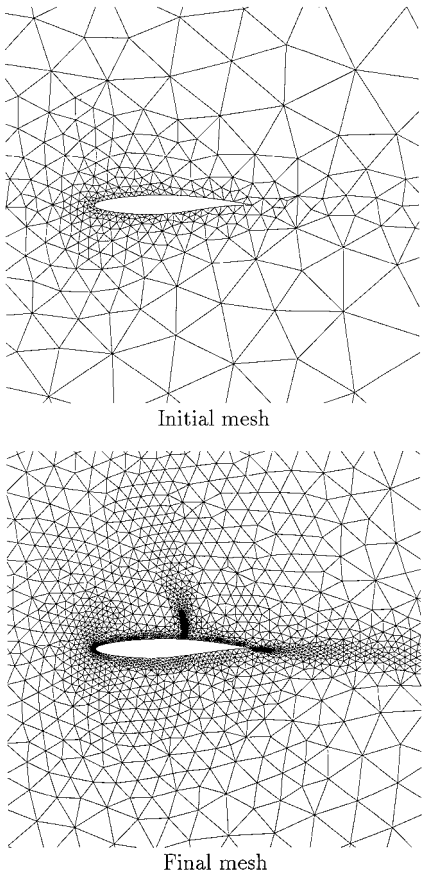

Fig. 11 Detail of the meshes near the airfoil.

Figure 9 presents contours of k and ϵ and their logarithms obtained on the final mesh. Several observations can be made: The fields of $\mathcal{K} = \ell n(k)$ and $\mathcal{E} = \ell n(\epsilon)$ present gentler variations than those of k and ϵ, an indication that discretization of logarithms results in a more accurate approach. Also the fronts in $\mathcal{K}$ and $\mathcal{E}$ are not as steep as those in k and ϵ except perhaps across the shock. This is especially true for ϵ, which is very large near the leading-edge stagnation point (dimensionless value of order 2, whereas it is of order 10^{-8} in the freestream). Note also that close to the leading edge there are points with very small values of ϵ, but for which the eddy viscosity is important. In such a region, even small errors for ϵ may have disastrous effects on the eddy viscosity. This difficulty is completely eliminated when the logarithms are used to compute the solution.

Finally, Fig. 10 presents a comparison of predicted values of the pressure coefficient with experimental measurements.[32] As can be seen, the agreement with the experimental data improves with adaptivity. Results on mesh 3 are grid converged.

C. Transonic Flow over an RAE2822 Airfoil

The flow over an RAE2822 airfoil is computed at a Mach number $M = 0.725$, $\alpha = 2.54$ deg, and a Reynolds number $Re = 6.5 \times 10^6$. Four cycles of adaptation are performed. Details of the initial and final meshes near the airfoil are shown in Fig. 11. Note the extreme clustering in the boundary layer and in the wake, as well as near the shock on the upper side of the airfoil. The pressure distribution on the first and final adapted meshes is shown in Fig. 12. The solution accuracy improves significantly between these meshes. Finally, predictions of the pressure coefficient along the airfoil are compared with measurements[32] in Fig. 13. The agreement improves steadily with adaptation. However, the shock is sharper than measured, probably due to the use of wall functions, which do not account for the

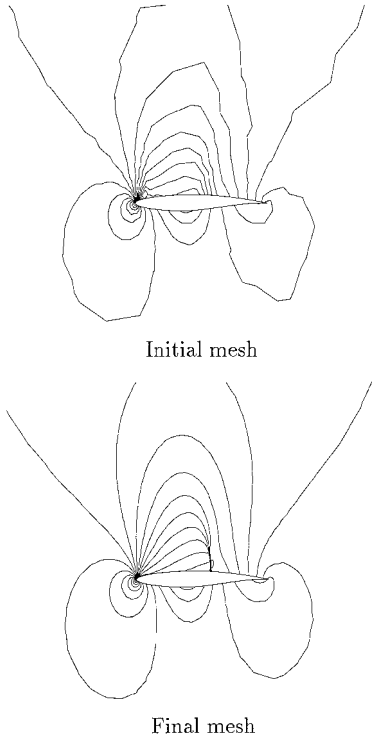

Fig. 12 Pressure distribution.

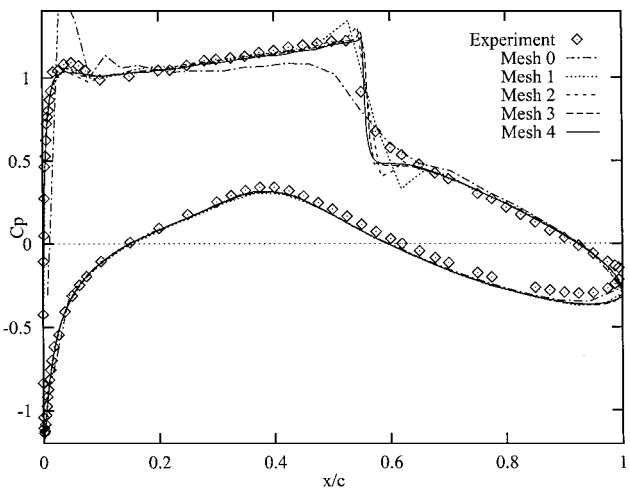

Fig. 13 Distribution of the pressure coefficient on the airfoil.

viscous subsonic layer near the wall. Comparison of predictions on meshes 3 and 4 indicate grid converged results.

VII. Conclusion

This paper presents the use of logarithmic variables for adaptive solution of compressible turbulent flows. The use of logarithmic variable guarantees positivity of turbulence variables throughout the domain and through the course of iterations. This increases the robustness of the solver.

The logarithmic variable formulation makes it possible to obtain solutions on coarse initial meshes. Because the logarithms vary more slowly than their arguments, accuracy is improved near sharp fronts. Furthermore, accuracy in regions of low-turbulence level is also improved because divisions by small quantities are eliminated.

The adaptive procedure uses error estimates in all field variables including the eddy viscosity. Hence, adaptivity reacts to shocks, shear layers, stagnation points, boundary layers, and wakes. This results in improved accuracy for all field variables.

The methodology was validated on a case possessing a closed-form analytic solution. Adaptive predictions indicate good agreement with measurement for the airfoils considered. However, shock predictions are sharper than measurements. This is probably due to the use of wall functions that do not account for shock–boundary-layer interactions. Adaptivity is a simple tool to perform adaptive grid refinement studies leading to grid independent predictions.

Acknowledgments

This work was supported in part by the Natural Sciences and Engineering Research Council, Canada; the Fonds de Formation de Chercheurs et d'Aide à la Recherche; and U.S. Air Force Office of Scientific Research Grant F49620-96-1-0329.

References

[1]Lee, D., van Leer, B., and Lyn, J. F., "A Local Navier–Stokes Preconditioner for all Mach and Cell Reynolds Numbers," *Proceedings of the AIAA 13th Computational Fluid Dynamics Conference*, AIAA, Reston, VA, 1997, pp. 842–855 (AIAA Paper 97-2024).

[2]Nichols, R. H., "Development and Validation of a Two-Equation Turbulence Model with Wall Functions for Compressible Flow," AIAA Paper 96-2385, June 1996.

[3]Suhs, N. E., Nichols, R. H., and Denny, A. G., "Unsteady Viscous Flow Computations Using a Two-Equation Turbulence Model with Wall Functions for Compressible Flow," AIAA Paper 96-2430, June 1996.

[4]Schonfeld, T., Colin, O., and Rudgyard, M., "Parallel Implementation of a k–ϵ Turbulence Model with Wall Functions for Unstructured Grids," AIAA Paper 96-2061, June 1996.

[5]Ilinca, F., "Méthodes d'éléments finis adaptatives pour les écoulements turbulents," Ph.D. Thesis, Mechanical Engineering Dept., École Polytechnique of Montréal, Montreal, PQ, Canada, March 1996.

[6]Ilinca, F., and Pelletier, D., "Positivity Preservation and Adaptive Solution for the k–ϵ Model of Turbulence," *AIAA Journal*, Vol. 36, No. 1, 1998, pp. 44–50.

[7]Ilinca, F., Hétu, J.-F., and Pelletier, D., "A Unified Finite Element Algorithm for Two-Equation Models of Turbulence," *Computers and Fluids*, Vol. 27, No. 3, 1998, pp. 291–310.

[8]Luo, H., Baum, J., and Lohner, R., "Computation of Compressible Flows Using a Two-Equation Turbulence Model on Unstructured Grids," AIAA Paper 97-0430, Jan. 1997.

[9]Peraire, J., Vahdati, M., Morgan, K., and Zienkiewicz, O. C., "Adaptive Remeshing for Compressible Flow Computations," *Journal of Computational Physics*, Vol. 72, No. 2, 1987, pp. 26–37.

[10]Palmério, B., and Dervieux, A., "2D and 3D Unstructured Mesh Adaption Relying on Physical Analogy," *Proceedings of the Second International Conference on Numerical Grid Generetion in CFD*, 1988.

[11]Fortin, M., Vallet, M. G., Poirier, D., and Habashi, W. G., "Error Estimation and Directionally Adaptive Meshing," AIAA Paper 94-2211, June 1994.

[12]Becker, R., and Rannacher, R., "A Feed-Back Approach to Error Control in Finite Element Methods: Basic Analysis and Examples," *East-West Journal of Numerical Mathematics*, Vol. 4, No. 4, 1996, pp. 237–264.

[13]Zienkiewicz, O. C., and Zhu, R., "A Simple Error Estimator and Adaptive Procedure for Practical Engineering Analysis," *International Journal for Numerical Methods in Engineering*, Vol. 24, No. 2, 1987, pp. 337–357.

[14]Wu, J., Zhu, J., Szmelter, J., and Zienkiewicz, O. C., "Error Estimation and Adaptivity in Navier–Stokes Incompressible Flows," *Computational Mechanics*, Vol. 6, No. 3, 1990, pp. 259–270.

[15]Zienkiewicz, O. C., and Zhu, J. Z., "The Superconvergent Patch Recovery and A Posteriori Error Estimators. Part 1: The Recovery Technique," *International Journal for Numerical Methods in Engineering*, Vol. 33, No. 7, 1992, pp. 1331–1364.

[16]Ainsworth, M., Zhu, J., Craig, A., and Zienkiewicz, O., "Analysis of the Zienkiewicz–Zhu A-Posteriori Error Estimator," *International Journal for Numerical Methods in Engineering*, Vol. 28, 1989, pp. 2161–2174.

[17]Ainsworth, M., and Oden, J. T., "A Posteriori Error Estimation in Finite Element Analysis," *Computer Methods in Applied Mechanics and Engineering*, Vol. 142, No. 1, 1997, pp. 1–88.

[18]Launder, B. E., and Spalding, D. B., *Mathematical Models of Turbulence*, 6th ed., Academic, London, 1972.

[19]Ilinca, F., and Pelletier, D., "A Pressure Based Adaptive Finite Element Algorithm for Compressible Viscous Flows," AIAA Paper 96-0679, Jan. 1996.

[20]Ilinca, F., and Pelletier, D., "A Unified Approach for Adaptive Solution of Compressible and Incompressible Flows," AIAA Paper 97-0330, Jan. 1997.

[21]Pelletier, D., Ilinca, F., and Hétu, J.-F., "Adaptive Finite Element Method for Turbulent Flow near a Propeller," *AIAA Journal*, Vol. 32, No. 11, 1994, pp. 2186–2193.

[22]Pelletier, D., and Ilinca, F., "Adaptive Remeshing for the k–ϵ Model of Turbulence," *AIAA Journal*, Vol. 35, No. 4, 1997, pp. 640–646.

[23]Ilinca, F., Pelletier, D., and Garon, A., "An Adaptive Finite Element Method for a Two-Equation Turbulence Model in Wall Bounded Flows,"

International Journal for Numerical Methods in Fluids, Vol. 24, No. 1, 1997, pp. 101–120.

[24]Ilinca, F., Pelletier, D., and Arnoux-Guisse, F., "An Adaptive Finite Element Scheme for Turbulent Free Shear Flows," *International Journal for Computational Fluid Dynamics*, Vol. 8, No. 3, 1997, pp. 171–188.

[25]Sarkar, S., and Lakshmanan, B., "Application of a Reynolds Stress Turbulence Model to the Compressible Shear Layer," *AIAA Journal*, Vol. 29, No. 5, 1991, pp. 743–749.

[26]Zeman, O., "Dilation Dissipation: The Concept and Application in Modeling Compressible Mixing Layer," *Physics of Fluids A*, Vol. 2, No. 2, 1990, pp. 178–188.

[27]Arpaci, V., and Larsen, P., *Convection Heat Transfer*, Prentice–Hall, Englewood Cliffs, NJ, 1984.

[28]Ignat, L., Pelletier, D., and Ilinca, F., "An Adaptive Finite Element Method for Turbulent Heat Transfer," AIAA Paper 96-0607, Jan. 1996.

[29]Vemaganti, G., and Prabhu, R., "Application of a Two-Equation Turbulence Model for High Speed Compressible Flows Using Unstructured Grids," 24th AIAA Fluid Dynamics Conf., 1993.

[30]Lohner, R., Morgan, K., and Zienkiewicz, O. C., "Adaptive Grid Refinement for the Compressible Euler Equations," *Accuracy Estimates and Adaptive Refinements in the Finite Element Computations*, edited by I. Babuška, O. C. Zienkiewicz, J. Gago, and E. de Olievera, Wiley, New York, 1986, p. 393.

[31]de Sampaio, P. A. B., Lyra, P. R. M., and Weatherill, N. P., "Petrov–Galerkin Solutions of the Incompressible Navier–Stokes Equations in Primitive Variables with Adaptive Remeshing," *Computer Methods in Applied Mechanics and Engineering*, Vol. 106, No. 2, 1993, pp. 143–178.

[32]Advisory Group for Aerospace Research and Development, "Experimental Data Base for Computer Program Assessment," AR-138, AGARD.

P. Givi
Associate Editor